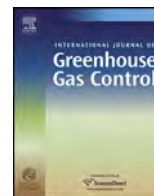




Contents lists available at ScienceDirect

International Journal of Greenhouse Gas Control

journal homepage: www.elsevier.com/locate/ijggc



Detection of CO₂ leakage from a simulated sub-seabed storage site using three different types of pCO₂ sensors

Dariia Atamanchuk^{a,*}, Anders Tengberg^{a,b}, Dmitry Aleynik^c, Peer Fietzek^{d,e},
Kiminori Shitashima^f, Anna Lichtschlag^g, Per O.J. Hall^a, Henrik Stahl^{c,h}

^a Department of Chemistry and Molecular Biology, Marine Chemistry, University of Gothenburg, SE-41296 Gothenburg, Sweden

^b Aanderaa Data Instruments AS, Midtun, NO-5828 Bergen, Norway

^c Scottish Association for Marine Science, Scottish Marine Institute, Argyll, Oban, PA37 1QA, UK

^d GEOMAR Helmholtz Centre for Ocean Research, 24148 Kiel, Germany

^e CONTROS Systems and Solutions GmbH, 24148 Kiel, Germany

^f International Institute for Carbon-Neutral Energy Research, Kyushu University, 744 Moto-oka, Nishi-ku, Fukuoka 819-0395, Japan

^g National Oceanography Centre Southampton, University of Southampton Waterfront Campus, European Way, Southampton, SO14 3ZH, UK

^h Zayed University, P.O. Box 19282, Dubai, United Arab Emirates

ARTICLE INFO

Article history:
Available online xxx

Keywords:
CCS
QICS
CO₂ release
Leakage detection
pCO₂ sensors

ABSTRACT

This work is focused on results from a recent controlled sub-seabed *in situ* carbon dioxide (CO₂) release experiment carried out during May–October 2012 in Ardmucknish Bay on the Scottish west coast. Three types of pCO₂ sensors (fluorescence, NDIR and ISFET-based technologies) were used in combination with multiparameter instruments measuring oxygen, temperature, salinity and currents in the water column at the epicentre of release and further away. It was shown that distribution of seafloor CO₂ emissions features high spatial and temporal heterogeneity. The highest pCO₂ values (~1250 μatm) were detected at low tide around a bubble stream and within centimetres distance from the seafloor. Further up in the water column, 30–100 cm above the seabed, the gradients decreased, but continued to indicate elevated pCO₂ at the epicentre of release throughout the injection campaign with the peak values between 400 and 740 μatm. High-frequency parallel measurements from two instruments placed within 1 m from each other, relocation of one of the instruments at the release site and 2D horizontal mapping of the release and control sites confirmed a localized impact from CO₂ emissions. Observed effects on the water column were temporary and post-injection recovery took <7 days.

A multivariate statistical approach was used to recognize the periods when the system was dominated by natural forcing with strong correlation between variation in pCO₂ and O₂, and when it was influenced by purposefully released CO₂.

Use of a hydrodynamic circulation model, calibrated with *in situ* data, was crucial to establishing background conditions in this complex and dynamic shallow water system.

© 2014 Elsevier Ltd. All rights reserved.

1. Introduction

Carbon Capture and Storage (CCS) is a method of capturing CO₂ from large point emitters, such as fossil fuel based power plants and heavy industry, and its sequestration into geological storage sites, e.g. deep geological formations covered by sealing caprock. This approach has been suggested as a potentially significant mitigation strategy to counteract climate change and ocean acidification

(Gough and Shackley, 2005; Haszeldine, 2009; Wilkinson et al., 2013).

Before sub-sea CO₂ storage can be carried out on a commercial scale, ecological consequences as well as adverse environmental and human impacts of potential CO₂ leakages need to be identified and reliable monitoring strategies for detection and quantification of potential leakages, both acute (broken pipes, leaking connections, etc.) and chronic (faults in the geological caprock), need to be developed.

Previous efforts to study either controlled or natural CO₂ releases with the focus on environmental impact and detectability were restricted to small-scale direct injections of liquid CO₂ into the deep water layers, observations of natural CO₂ seepage

* Corresponding author. Tel.: +1 902 494 4382.
E-mail address: Dariia.Atamanchuk@Dal.Ca (D. Atamanchuk).

sites and model studies of the fate of released CO₂. Small-scale liquid CO₂ injections were carried out in a series of experiments off the coast of California (Brewer, 2003, Brewer et al., 2004), which later developed into the FOCE (Free Ocean CO₂ Enrichment) program (Kirkwood et al., 2005, 2009; Walz et al., 2008). Natural marine CO₂ seepage sites, like the ones off the coast of Aeolian Islands Panarea and Vulcano, Southern Italy (Vizzini et al., 2010; Caramanna et al., 2011; Pearce et al., 2014) and Ischia island, Gulf of Naples, Italy (Hall-Spencer et al., 2008), are widely and extensively studied in terms of assessment of CO₂ impacts to seawater chemistry and ecology. Modelling studies based on natural CO₂ releases in Kagoshima Bay described physico-chemical processes of CO₂ transformation in seawater (Dissanayake et al., 2012). Numerous models were developed to predict the behaviour of leaking CO₂, purposefully stored under the seabed (Blackford et al., 2008; Kano et al., 2010; Dewar et al., 2013), and as a consequence the rise of pCO₂ (Kano et al., 2009) or the transformation pathways of released CO₂ in the deep ocean (Jeong et al., 2010).

Within the NERC funded research project QICS (Quantifying and Monitoring Potential Ecosystem Impacts of Geological Carbon Storage) a large scale controlled *in situ* CO₂ sub-seabed release was conducted in Ardmucknish Bay, Scotland (Fig. 1) in spring–summer of 2012, in order to make a simulation of a realistic CO₂ leakage event. An overview of the physical aspects of CO₂ migration through the sediment overburden and overlying water column, as well as of the ecological and biogeochemical impacts on the benthos, of this experiment were recently described in Blackford et al. (2014).

This paper focuses on challenges and technical aspects of detecting CO₂ emissions in the overlying water from this shallow water release experiment, using three different types of pCO₂ sensors in combination with standard hydrographical instrumentation for additional properties of seawater.

In this study we address the following questions:

How much did the CO₂ release affect the pCO₂ in the water column at different distances from the source and how did it compare to background natural variability? What was the spatial and temporal heterogeneity of the CO₂ plume in the water column during the release, and how quick was the recovery after the termination of the release? What parameters need to be measured in order to explain and model the changes in the carbonate system caused by CO₂ release? Which technical solutions for monitoring systems at storage sites, fixed and movable, would allow detection and/or identification CO₂ leakages with the highest probability?

2. Materials and methods

2.1. Study site and CO₂ release experiment

The CO₂ release experiment (QICS) was carried out in Ardmucknish Bay, near Oban on the Scottish west coast (Fig. 1, inset). After identification of a suitable site in the vicinity of the Scottish Association for Marine Science (SAMS, Dunstaffnage, Oban) (Taylor et al., in this issue), a thorough baseline survey was conducted during autumn of 2011 and in early 2012. The latter included a combination of acoustic surveys, sediment coring and diver-based characterization of background conditions prior to drilling and injection of CO₂.

In the beginning of 2012 (February–April), a southerly facing borehole was drilled, using a directional drilling rig, through the bedrock and terminating 10 m horizontally into unconsolidated sediments 350 m offshore in the northern part of the bay (Fig. 2a; see also <https://www.youtube.com/watch?v=bhmCGcEenjk> and Supplementary material: Video 1).

The CO₂ gas was released from a land-based container, through a 20 mm diameter welded stainless steel pipeline terminating in a

5 m long diffuser with multiple 0.5 mm perforations located 11 m below the seabed. The overlying water depth at the study site was 10–12 m depending on the tide. The injection phase started on May 17th and lasted for 37 days (day 0 to 36) until June 22nd, followed by the recovery period, until November 1st. CO₂ injection rates commenced at 10 kg CO₂ d⁻¹ at day 0, increasing to 83 kg CO₂ d⁻¹ by day 3, 150 kg CO₂ d⁻¹ at day 23 and 210 kg CO₂ d⁻¹ on day 33 (Fig. 3a). The total injected CO₂ amounted to 4.2 tonnes over the 37-day period.

Four zones with biogeochemically and ecologically similar characteristics were chosen: Zone 1 (Z1) was the epicentre of the release; Z2 and Z3 were 25 and 75 m distant from the epicentre respectively; Z4 was the control site at 450 m from the epicentre (Fig. 1). All zones were situated along the 10 m isobath. During the release phase up to 35 (depending on the injection rate and tides) individual bubble streams were observed by scuba divers at the epicentre of the release (Z1) rising from the sediment into the water column above it (https://www.youtube.com/watch?v=N.CUdiI5_r4 and Supplementary material: Video 2). The control site (Z4) was assumed to be unaffected by the CO₂ release. For further details on the experimental methodology see Taylor et al. (in this issue).

2.2. Instruments and sensors

Instruments' deployment and maintenance at the release site in Ardmucknish Bay during the experiment were undertaken by scuba diving, assuring precise positioning and handling of the equipment. Boat-deployed water column sampling and profiling (5 L Niskin bottle and SBE19 CTD from Seabird Inc.) was done from R/V Soel Mara using the onboard winch.

Tidal information and relevant weather data (solar radiation, wind speed and direction, precipitation and atmospheric pressure) were obtained at hourly interval from Poltips software and from the permanently installed weather stations at SAMS, and at nearby Dunstaffnage, respectively. To facilitate the wind pattern analysis, high resolution (2 km grid) Atmospheric WRF model was run over West Scotland for period of the CO₂ experiment.

In the work presented here data collected by four different types of instruments (a–d) was used (see Table 1 for deployment details).

(a) A Seaguard[®] autonomous datalogger from Aanderaa Data Instruments, www.aanderaa.com, (Fig. 2b) was fitted with a single point Doppler Current Meter (Victoria, 2011), a temperature and a conductivity/salinity probe, an oxygen optode (Tengberg et al., 2006) and a new type of pCO₂ optode recently described in Atamanchuk et al. (2014). In short, CO₂ gas diffuses from the surrounding water through a gas-permeable membrane into the sensing layer of the pCO₂ optode, where as a consequence the pH is modified. The magnitude of pH change is correlated to the pCO₂ level outside the membrane. The embedded Dual Lifetime Referencing (DLR) material exhibits a pH dependent fluorescence change, which is detected as a phase shift value of returning red light. Response time (τ_{63}) is between 45 s (at 40 °C) and 4.5 min (at 0 °C). Observed precision of the sensors is $\pm 2\text{--}3 \mu\text{atm}$ and absolute accuracy is 2–75 μatm ; better accuracy is achievable through *in situ* calibration. Stability of the sensors during long-term deployments was shown to be longer than seven months (Atamanchuk et al., 2014).

The pCO₂ optode was calibrated before the deployment at 40 points (10 pCO₂ concentrations and four temperatures) using a temperature controlled water bath that was bubbled with different gas mixtures. In addition the 3-D calibration plane was adjusted *in situ* using one-point referencing methodology (Atamanchuk et al., 2014) and a reference value from a water sample taken on day 14 of the release experiment. This value was assumed to represent the background pCO₂ even though it was taken before the actual measurements of the optode commenced (day 18). Following water

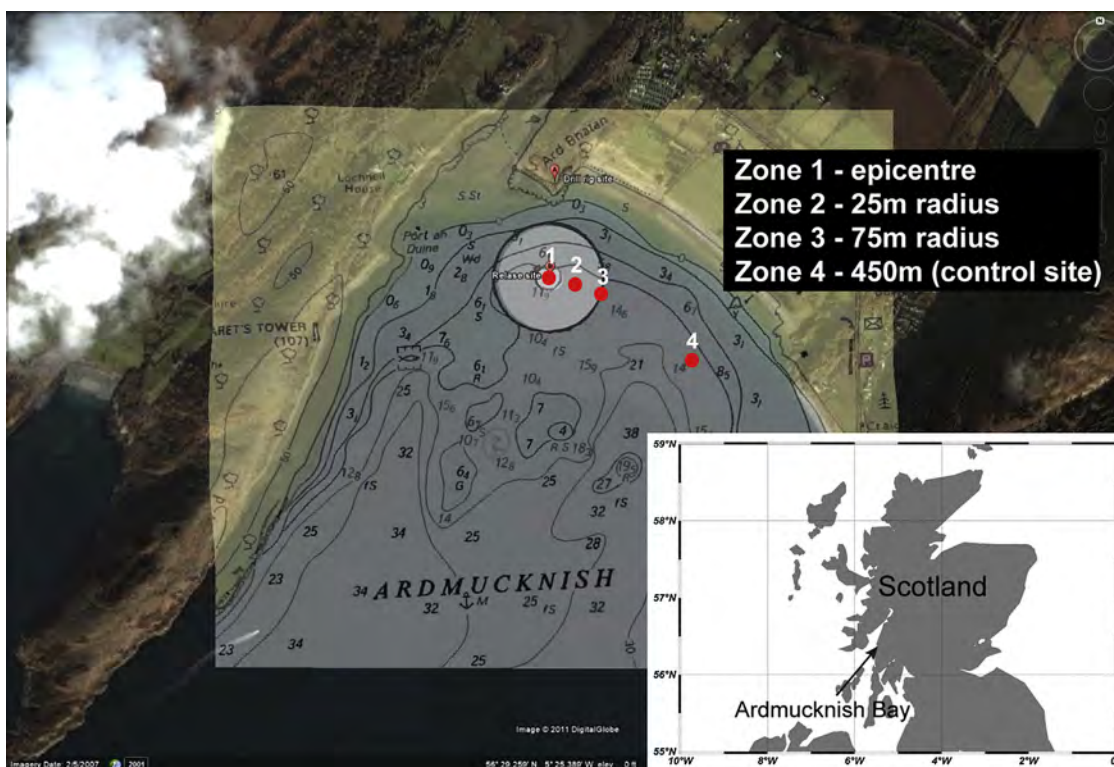


Fig. 1. Satellite picture of Ardmucknish Bay (<https://maps.google.com>) where the release of CO₂ gas took place with indication of sampling sites (red circles) at Zones 1–4. *Inset:* The study site Ardmucknish Bay, Oban, Scotland on the map. (For interpretation of the references to colour in this figure legend, the reader is referred to the web version of this article.)

samples' data served as a reference for subsequent accuracy control (Fig. 4a, Table 2).

Based on factory specifications the absolute accuracies for data from other sensors presented here were estimated to be: $\pm 1\%$ for current speed measurements, $\pm 5^\circ$ for current direction, $\pm 0.05^\circ\text{C}$ for temperature and ± 0.05 for salinity. The oxygen optode was saturation checked against atmospheric values in-between deployments; the absolute accuracy was estimated to be $\pm 3\%$.

None of the Seaguard[®] sensors demonstrated detectable drift (within sensor specifications) during the five-months period that

the instrument was used in this project, and no major bio-fouling was noticed at the five occasions that the instrument was lifted, cleaned and redeployed.

The Seaguard[®] instrument was anchored to the bottom by burying the housing halfway into the sediment (Fig. 2b) with the sensors measuring every 15 min ~ 30 cm above the seabed. The instrument was recovered, inspected for damages, cleaned, its data downloaded and it was subsequently redeployed at five separate occasions (Table 1) during the QICS experiment. Each time the instrument was redeployed, it was placed as close as possible to

Table 1
Summary of the deployments and instruments used in this study.

Instrument deployment	Measuring parameters	Period (dd.mm.)	Zone	Measurement position (cm) (above the seafloor)	Water depth (m)
<i>Release phase</i>					
Seaguard.D1	pCO ₂ , O ₂ , C/T	04.06. to 12.06.	Z1	30	10–12
Seaguard.D2	pCO ₂ , O ₂ , C/T, currents	12.06. to 19.06.	Z1	30–40	10–12
Seaguard.D3 ^a	O ₂ , C/T, currents	19.06. to 22.06.	Z4	30–40	11–13
ISFET.D1	pCO ₂ , T	18.05. to 01.06.	Z1	3–5	10–12
ISFET.D2	pCO ₂ , T	05.06. to 25.06.	Z1	3–5	10–12
CONTROS.D1	pCO ₂ , C/T/D	22.06.	Z1 to Z4	0.3–1.8 ^b	9–11.5
RCM#419.D1	C/T, currents	09.05. to 18.06.	Z3	~ 80	11–13
<i>Release/recovery phase</i>					
Seaguard.D4	pCO ₂ , O ₂ , C/T, currents	22.06. to 29.06.	Z1	30–40	10–12
RCM#419.D2	C/T, current	18.06. to 29.06.	Z4	~ 80	11–13
RCM#643.D2	C/T, current	18.06. to 29.06.	BI ^c	~ 80	25–27
<i>Recovery phase</i>					
Seaguard.D5	pCO ₂ , O ₂ , C/T, currents	05.07. to 13.08.	Z1	30–40	10–12
Seaguard.D6	pCO ₂ , O ₂ , C/T, currents	17.09. to 29.10.	Z1	30–40	10–12
CONTROS.D2	pCO ₂ , C/T/D	27.06.	Z1 to Z4	0.8–3.3 ^b	11.1–13.6
RCM#419.D3	C/T, current	29.06. to 18.09.	Z4	~ 80	11–13
RCM#643.D3	C/T, current	29.06. to 18.09.	BI ^c	~ 80	25–27

^a pCO₂ sensor's protection cap left resulting in no data.

^b Measurement depth during drifting measurements.

^c Bay inlet.

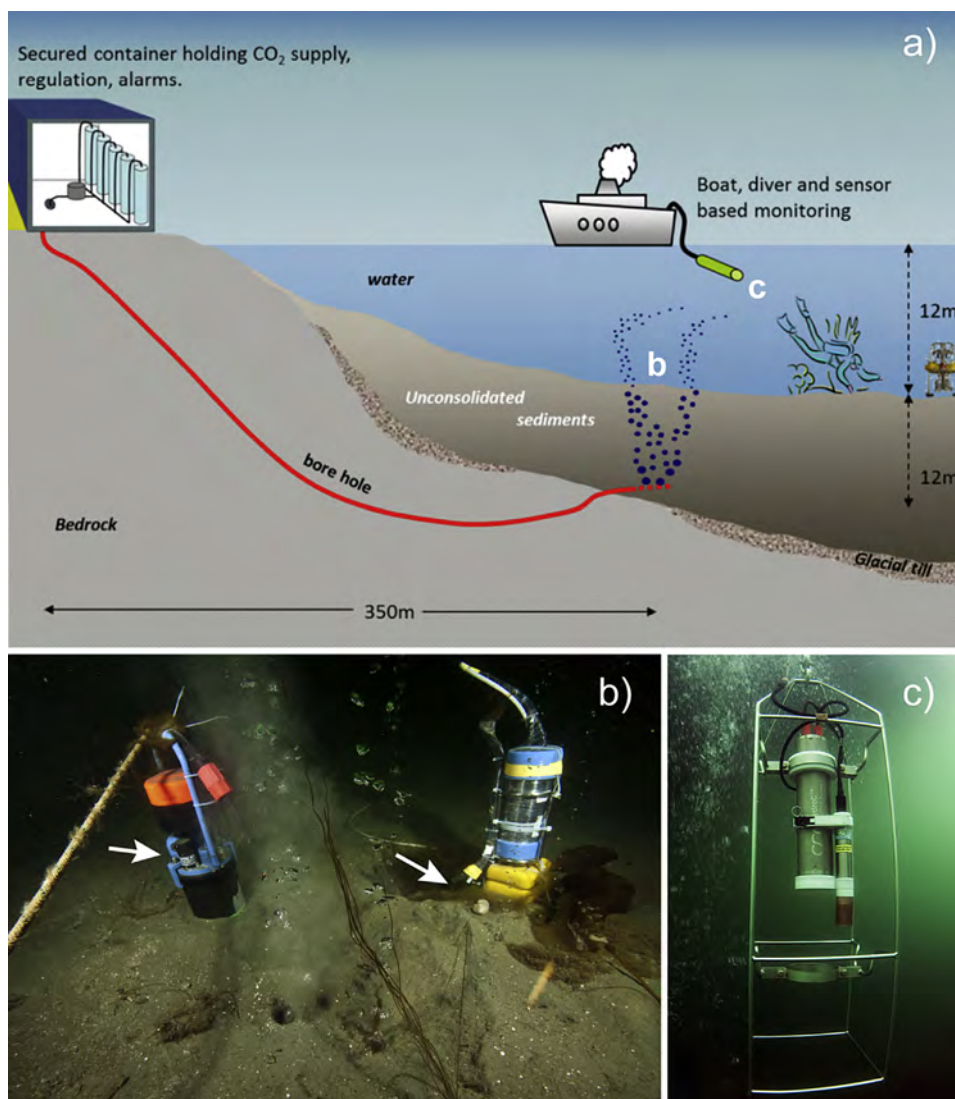


Fig. 2. (a) Schematic of the QICS *in situ* release experiment indicating the relative locations (b and c) of the $p\text{CO}_2$ sensors used in this study; (b) Photo of Seaguard® (left) and ISFET (right) $p\text{CO}_2$ sensors deployed *in situ* next to CO_2 bubble streams. White arrows indicate positions of sensors on the instruments, 30 and 3 cm above the bottom, respectively; (c) Underwater photo of the towed CONTROS HydroC™ $p\text{CO}_2$ sensor.

the same location at the release site (Z1). Gaps in data recorded with the instrument during five months of the project was either due to servicing, when the instrument was taken out of the water for few hours, or because it was used in other projects, i.e. long gap between deployments four and five (Table 1, Fig. 4). On one deployment (Seaguard.D3, see Table 1), the $p\text{CO}_2$ sensor protection cap was left on by mistake while deployed at Z4, and hence the data were excluded from further analysis.

(b) A cabled on-line ion-sensitive field-effect transistor (ISFET) based (e.g. Shitashima and Kyo, 1998; Shitashima et al., 2002; Martz et al., 2010) pH/ $p\text{CO}_2$ sensor (Shitashima et al., 2008; Shitashima, 2010) was deployed at the epicentre (Fig. 2b). The ISFET based pH sensor uses an ion-sensitive field-effect transistor as the pH electrode, and a chloride ion selective electrode (CI-ISE) as the reference electrode. The ISFET is a semiconductor made of p-type silicon coated with SiO_2 , with Si_3N_4 as the gate insulator surface that is the ion-sensing layer. In aqueous media, the interface potential between the reference electrode and the sensing layer is a function of the activity of the H^+ ion, i.e. pH. The CI-ISE is a pellet made of several metal chlorides having a response to the chloride ion, a major element in seawater. The electric potential of the CI-ISE is stable in the seawater, since it has no inner electrolyte solution.

The devised pH sensor shows quick response time ($\tau_{90} < 1$ s) with high accuracy (± 0.005 pH).

The principle of $p\text{CO}_2$ measurement using ISFET-pH technology is as follows. Both the ISFET-pH electrode and the CI-ISE of the pH sensor are sealed in a unit with a gas permeable membrane whose inside is filled with inner electrolyte solution with 1.5% of NaCl. The pH sensor can measure changes in $p\text{CO}_2$ from changes in the pH of the inner solution, which is caused by penetration of CO_2 through the membrane. An amorphous Teflon membrane (Teflon AF™) manufactured by DuPont was used as the gas permeable membrane. The *in situ* (3000 m depth, 1.8 °C) response time (τ_{90}) for detecting changes in $p\text{CO}_2$ was <60 s (Shitashima et al., 2013). Response time of ISFET sensor at the conditions of this experiment was not estimated.

The $p\text{CO}_2$ sensor data were calibrated *in situ* on day 2 of the gas release and on day 5–6 using baseline values. *In situ* calibration involved correction of an existing laboratory calibration of the pH/ $p\text{CO}_2$ sensor (not shown in this paper) and the data (depth, temperature, salinity and A_T) of reference bottom water samples (see Section 2.3). Since background $p\text{CO}_2$ showed daily oscillation, we determined a linear regression of the raw $p\text{CO}_2$ sensor data vs. calculated baseline $p\text{CO}_2$ data, which was used for correction of all the

raw ISFET- $p\text{CO}_2$ data before presenting it here (Shitashima et al., 2013).

(c) A HydroCTM – CO_2 sensor from CONTROS Systems and Solutions, GmbH, www.contros.eu (Saderne et al., 2013, Fiedler et al., 2013, Fietzek et al., 2014) was deployed twice for profiling and towed measurements in the water column (Table 1). Data for 2D $p\text{CO}_2$ mapping of the sites Z1 through Z4 was collected during the final day of the gas release (day 36) and 5 days after the gas was switched off (day 41). The sensor was towed behind the vessel at 0.1–0.2 knts ~1 m above the bottom along transect from Z1 to Z4. In between the different zones it was heaved and veered by winch at 0.1 m/s.

The HydroCTM determines the $p\text{CO}_2$ in water at an accuracy of better than $\pm 1\%$ by NDIR absorption measurements within an internal headspace realized by means of a flat membrane equilibrator (Fietzek et al., 2014). The sensor was factory calibrated in water just before and after the two deployments at an *in situ* temperature of 11 °C for a range of 200–1700 μatm (Fietzek et al., 2014). The field data was drift corrected by considering the information from the regular sensor zeroings as well as the pre- and the post-deployment calibration of the sensor. Data was processed as described in Fietzek et al. (2014), with the transformation of the two polynomials being carried out based on sensor runtime. All sensor zeroings and subsequent 5 min flush intervals were removed from the data set for response time determination and correction (Fiedler et al., 2013). The sensor's response times were determined automatically from the recovery of the corrected $p\text{CO}_2$ signals within the flush intervals, neglecting the initial $p\text{CO}_2$ values representing gas mixing artefacts within the internal gas stream (Fiedler et al., 2013). An average response time (τ_{63}) of 84 s with a standard deviation of ± 4.2 s was derived from a total of six flush intervals during deployment. Since the sensor only experienced a maximum temperature difference of 1 °C between all sensor zeroings and the maximum deployment depth was less than 15 m, both temperature and depth influence on the response time were neglected and a constant response time was assumed for further processing. Using a numerical inversion algorithm the data was finally corrected for the time-lag influence caused by the sensor's time constant (Miloshevich et al., 2004). Different averaging methods were applied to the data prior to the response time correction depending on whether the correction was used to enhance temporal resolution of events or to minimize noise amplification caused by the processing algorithm.

(d) To obtain more background data on currents, salinity and temperature two RCM9 instruments from Aanderaa Data

Instruments, www.aanderaa.com, were also deployed and relocated in the area at several occasions (Table 1).

2.3. Discrete water samples

For values of dissolved inorganic carbon (DIC) and total alkalinity (A_T) in the bottom water a series of discrete samples was collected by boat in 5 L Niskin bottles 1 m above the bottom (Table 2). These samples were analysed for DIC and A_T in the lab using standard techniques. For DIC analysis samples were measured with an Apollo SciTech DIC analyzer (AS-C3), which uses a LI-COR $\text{CO}_2/\text{H}_2\text{O}$ (LI-7000) infrared analyser to detect the CO_2 released from the samples after acidification with a 10% H_3PO_4 solution. Precision of DIC measurements was calculated as the standard deviation between four and five readings of the same sample and the average value was 3.3 $\mu\text{mol kg SW}^{-1}$. Potentiometric titration and subsequent Gran evaluation was used for A_T samples (Dickson et al., 2003). Since A_T samples were run without duplicates, precision of the method was calculated as a standard deviation between the readings of Certified Reference Material (CRM) during the day of analysis and was estimated to be 2.8 $\mu\text{mol kg SW}^{-1}$. Accuracies of both DIC and A_T measurements were set to 0.5 $\mu\text{mol kg SW}^{-1}$ by regular analysis of CRM. For comparison with *in situ* sensor data, the DIC and A_T data were converted into $p\text{CO}_2$ with an overall uncertainty of $\pm 10 \mu\text{atm}$ using the CO2SYS software (Lewis and Wallace, 1998) using *in situ* temperature and salinity from SBE19 CTD.

2.4. Multivariate data analysis

Recorded data from the Seaguard[®] of CO_2 release rate, gas release rates, tidal oscillations and meteorological parameters such as air and water temperature, wind direction and speed, precipitation and atmospheric pressure, was used for multivariate data analysis using SIMCA 13 software (Umetrics AB, www.umetrics.com). First, a Principal Component Analysis (PCA) was applied to each deployment dataset (Seaguard.D1–D2, D4–D6) to identify dependencies between the variables, such as $p\text{CO}_2$, oxygen, salinity, temperature, gas release rate (where applicable), tidal conditions and meteorological parameters. PCA usually serves for initial inspection of data for outliers, identifying significance of each factor based on a simple analysis tools (scatter and loadings plots, coefficients list, etc). After comparison of the patterns for the gas

Table 2

Summary of the reference $p\text{CO}_2$ data derived from discrete water samples at Z1 and Z4 vs. that measured by HydroCTM, $p\text{CO}_2$ optode and ISFET-based $p\text{CO}_2$ sensor at Z1. Number in brackets (in %) represents a relative change of the measured value against the baseline value at Z1, and the baseline value at Z4 (control) against the value at Z1 (epicentre).

Date (dd.mm.)/ Day of experiment	Baseline values		HydroC TM peak values (μatm)	Optode (μatm)	ISFET (μatm)	Tide	CO_2 release	Water samples at Z4 (μatm)
	Water samples at Z1 (μatm)	HydroC TM (μatm)						
31.05. day 14	369	–	–	–	461 (+25%)	Low	Yes	375 (+1.6%)
18.06. day 32	362	–	–	390 (+7.7%)	671 (+85%)	Low	Yes	345 (–4.7%)
22.06. day 36 (morning)	–	367 ^a	508(+38%) 538(+47%)	–	846 (+131%)	High–low	Yes	–
22.06. day 36 (afternoon)	–	362 ^a	479(+32%) 504(+39%) 737(+104%)	–	807 (+123%)	Low–high	Yes	–
27.06. day 41 (morning)	348	–	–	397 (+14%)	–	Low–high	No	376 (+8%)
27.06. day 41 (afternoon)	–	368 ^a	–	377 (+2.5%)	–	High–low	No	–
11.07. day 55	349	–	–	380 ^b (+8.9%)	–	High	No	360 (+3.2%)
18.09. day 90	373	–	–	342 (–8.3%)	–	Low	No	335 (–10%)

^a Data resembles averaged baseline values excluding peak values.

^b Data indicates the value measured closest to the time of water sampling for referencing.

release phase and recovery phase, conclusions about the response of the system to external CO₂ supply were made.

Based on the outcome from PCA, a Partial Least Squares (PLS) regression model was used to identify parameters, which contributed significantly to pCO₂ and oxygen variations both during the gas release (Seaguard.D1, .D2, .D4-release) and after it was cut off (Seaguard.D4-recovery, .D5, .D6). A supervised PLS model aimed to put pCO₂ and oxygen variations into a context of their correlation with each other and the relation to other parameters. For this pCO₂ and oxygen parameters were assigned in the model as Y variables or result variables, which depend on X variables, i.e. other measured parameters.

2.5. Hydrodynamic modelling

High resolution unstructured grid hydrodynamic model for Loch Etive and Ardmucknish bay, developed at SAMS (Aleynik et al., 2012), was used for modelling of the hydrodynamic conditions at the site. A major advantage of the Finite Volume Community Ocean Model (FVCOM) used here, is in its geometric flexibility, making it a suitable solution for hydrographical modelling along complex coastlines and bathymetry, such as off the West coast of Scotland. The model consists of 6601 horizontal non-overlapping triangular elements and 3776 vertices, with enhanced horizontal resolution (22 m) in the narrows and over the sills (Connel, Bon Awe). At the CO₂ release site, the model has an effective resolution of 120–180 m. In the vertical dimension, the model consists of 11 terrain following layers. FVCOM is a primitive-equation, free-surface, hydrostatic model described in detail in Chen et al. (2003). A model simulation was performed using real-world data—laterally it was forced with a set of CTD data from fixed platforms deployed around Ardmucknish Bay. Tidal forcing was calculated with 6 major tidal harmonics (M2, S2, N2, K2, O1, K1) for the nearest port in Oban, and the meteo-forcing parameters (short-wave and net heat flux, precipitation/evaporation, atmospheric pressure) have been derived from the Met-Office weather station at Dunstaffnage. Freshwater runoff was compiled using a lagged precipitation rate over the catchment area. The forecast parameters of the model include surface elevation, temperature, salinity, current velocity and with the dye-CO₂ module (Blackford et al., 2013) prediction of several components of the carbonate system – DIC concentration, pH and pCO₂ in seawater – is also possible (see Supplementary material).

3. Results

3.1. pCO₂ during gas release

Fig. 3a presents details of pCO₂ changes during the release phase, continuously measured with the two different independent sensors systems, i.e. pCO₂ optode and ISFET-pCO₂, along with the tidal conditions and gas release rates. Fig. 3b shows pCO₂ variations measured with optode and ISFET-pCO₂ in correlation with tidal circulation. Correlation between pCO₂ values measured by optode, HydroCTM-CO₂ sensor, ISFET-based sensor and water samples data is given in the Table 2. Fig. 3c highlights the redeployment of Seaguard[®] instrument at the release site and related to this event changes in pCO₂ and oxygen time-series.

A strong dependency between low tide and pCO₂ optode measurements was observed and is highlighted below in Section 3.4. A tidal relation was also visible from the ISFET based pH/pCO₂ sensor deployed about 1 m away from the Seaguard[®] (Fig. 3b). This sensor was placed ~3 cm above the seafloor, at the rim of one of the pockmark actively venting CO₂. Although having very similar baseline values, e.g. 356 ± 4 μatm for ISFET-pCO₂ sensor and 369 ± 7 μatm for pCO₂ optode during days 18–21 of CO₂ release, the ISFET-pCO₂ sensor showed generally higher amplitude pCO₂ peaks during low

tide (up to 420–900 μatm) comparing to the corresponding peaks from the pCO₂ optode (up to 400–580 μatm). Most of the tidally induced pCO₂ peaks from both the optode and ISFET sensors did concur, but not always (Fig. 3b).

The tidal pCO₂ peaks were not reflected at all in the data from discrete water samples collected randomly ~1 m above the seabed of the bubbling area in Z1. The water samples showed approximate baseline levels for pCO₂ at the release and resembled baseline levels at the control site within ±5–8% variation. Values of peak concentrations appeared as up to 131% higher above the baseline (Table 2). For example, water sample values showed 362 μatm on day 32, while optode and ISFET-pCO₂ detected 390 and 671 μatm, respectively.

Steep vertical and horizontal pCO₂ gradients were observed while towing the CONTROS HydroCTM sensor ~1 m above the bottom from Z1 to Z4 on day 36, the last day of the gas release. At the Z4 (control site) the sensor measured a pCO₂ of 368 ± 2 μatm without significant spatial heterogeneity. For Z2 and Z3 the same values were obtained, 363 ± 2 μatm, which were of comparable magnitude to those at the control site. When measuring closer to the epicentre in Z1, baseline values at the same depth were 367 ± 1 μatm and 362 ± 2 μatm in the morning and the afternoon, respectively. Sharp pCO₂ peaks of as high as 540 μatm and 740 μatm in the morning and the afternoon respectively, which corresponded to 47% and 104% higher above the baseline values (day 36, Table 2), were observed when the sensor was towed through the area with active venting of CO₂, i.e. within the ‘footprint’ of the gas release (Fig. 5a shows the afternoon data). At the same time ISFET-pCO₂ recorded 800–850 μatm closer to the bottom. Later during the same day, the pCO₂ optode recorded ~570 μatm pCO₂ 30 cm above the seabed and the ISFET-pCO₂ sensor showed as high as 1250 μatm at 3 cm above the seabed. The fact that HydroCTM detected higher peak values in the afternoon correlates with the tide dependency observed by the sensors deployed on the seabed. Low tide occurred at the site in conjunction with the afternoon measurements as can be seen in the lower water depth of Fig. 5a compared to Fig. 5b, which shows a transect of the same area obtained during high tide.

At two occasions distinct peaks in the HydroCTM signal even suggest detection of ascending gas bubbles in the water column (one example depicted in Fig. 5a at around 14:32). This observation was underlined by visual evidence of gas bubbles at the water surface around the same time. Moreover, the towed HydroCTM measurements showed distinct pCO₂ differences between the surface water and the bottom water (see Fig. 5b). It could be observed that these differences were influenced by tides and currents as they contributed to mixing of the entire water column within the experimental area, thus affecting the observed gradients (data not shown here).

3.2. pCO₂ during recovery period

ISFET-pCO₂ sensor showed values, which approached the background level, starting already from day 35 (one day before the gas was shut off) and levelled off at ~350 μatm on day 37. Actual release of CO₂ gas was stopped after day 36, which was followed by decline in the pCO₂ concentrations at the epicentre as detected by pCO₂ optode (Fig. 6). Within 7 days after terminating the gas flow, pCO₂ values had reached stable baseline partial pressure of ~345–355 μatm. The post-injection recovery pattern was also supported by data from discrete water samples (Table 2): DIC and A_T values increased by 75 and 105 μmol kg SW⁻¹ and stabilized at the levels of 2095 and 2213 μmol kg SW⁻¹, respectively (Fig. 6). As the relative increase in A_T is higher than the increase in DIC, pH shifts to higher values indicating a decrease in pCO₂. In Z1 the HydroCTM pCO₂ sensor measured on average 368 ± 2 μatm ~1 m above the

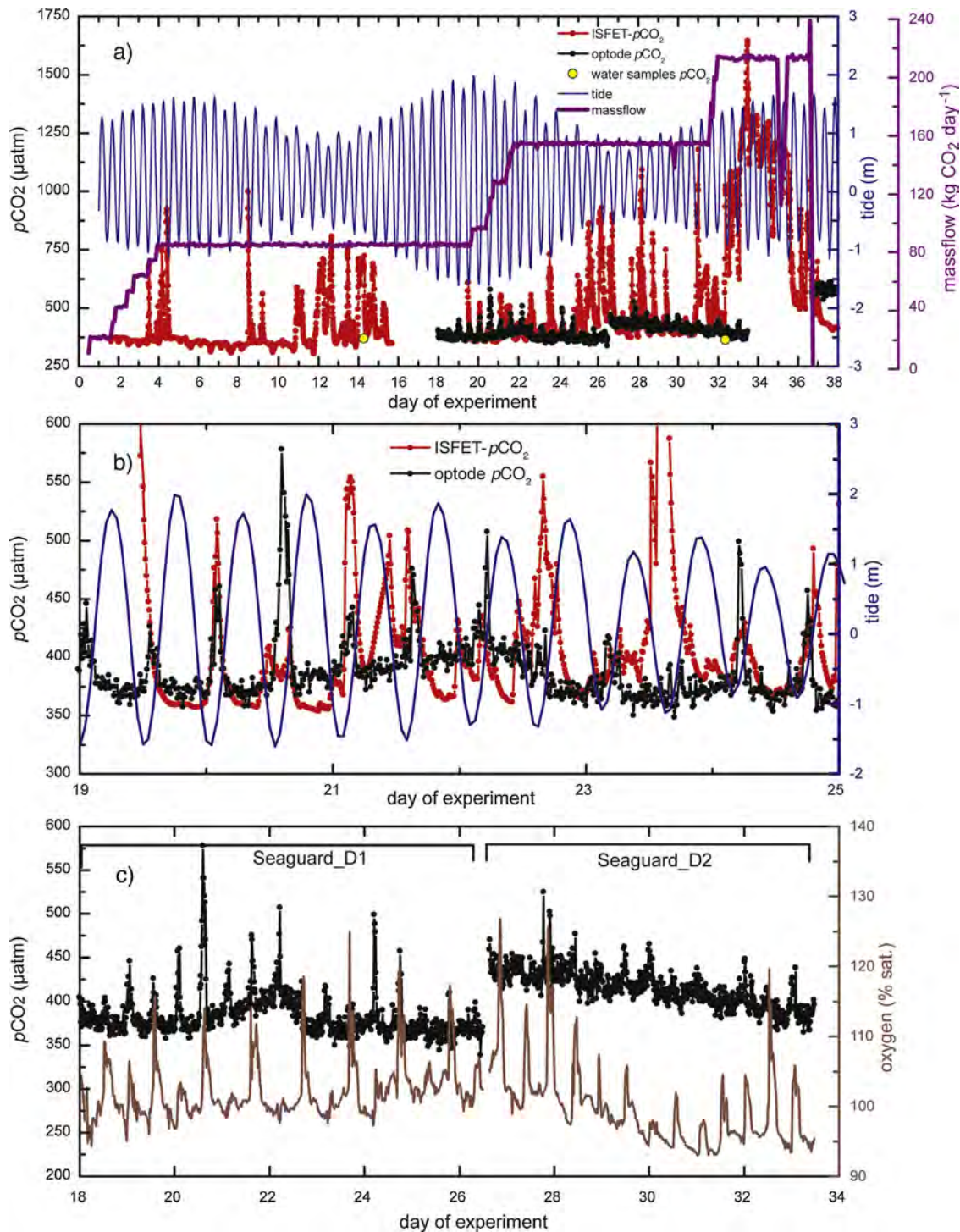


Fig. 3. Summary of data collected during the QICS campaign.(a) period of CO_2 release: $p\text{CO}_2$ data from optode (black line) is compared to ISFET- $p\text{CO}_2$ sensor (red) with respect to tidal variability (blue) and mass flow rate of CO_2 release (violet). Drop in the massflow rate between the days 35 and 36 was due to freezing of the system, which delivered CO_2 ; (b) correlation between the peaks in $p\text{CO}_2$ optode and ISFET- $p\text{CO}_2$ data and tidal circulation at Z1 during the release; (c) $p\text{CO}_2$ and oxygen time-series recorded during two deployments of the Seaguard® at the release site (Z1). A gap on day 26 indicates recovery and redeployment of the instrument. Spikes on both time-series are attributed to tidal cycles at the site. (For interpretation of the references to colour in this figure legend, the reader is referred to the web version of this article.)

bottom on the fifth day of recovery (day 41, Fig. 5b). With measured $p\text{CO}_2$ values of $369 \pm 2 \mu\text{atm}$, $368 \pm 2 \mu\text{atm}$ and $370 \pm 1 \mu\text{atm}$ for zones Z2, Z3 and Z4 respectively no significant spatial variation was detectable.

After recovery to background values, the partial pressure measured by the $p\text{CO}_2$ optode typically oscillated with $\pm 30 \mu\text{atm}$ around mean value of $\sim 360 \mu\text{atm}$. Comparison with the water

samples from Z1 showed the difference in the values within $\pm 8\text{--}9\%$ (day 55 and 90, Table 2). However, between August 2nd and 4th $p\text{CO}_2$ levels increased significantly with $\sim 100 \mu\text{atm}$ or $\sim 28\%$ compared to background values. A similar event happened during August 8th–9th and resulted in an additional rise in $p\text{CO}_2$ with $\sim 70 \mu\text{atm}$ or $\sim 19\%$ compared to background (Fig. 4a). Both these occasions coincided with distinct changes in the general circulation

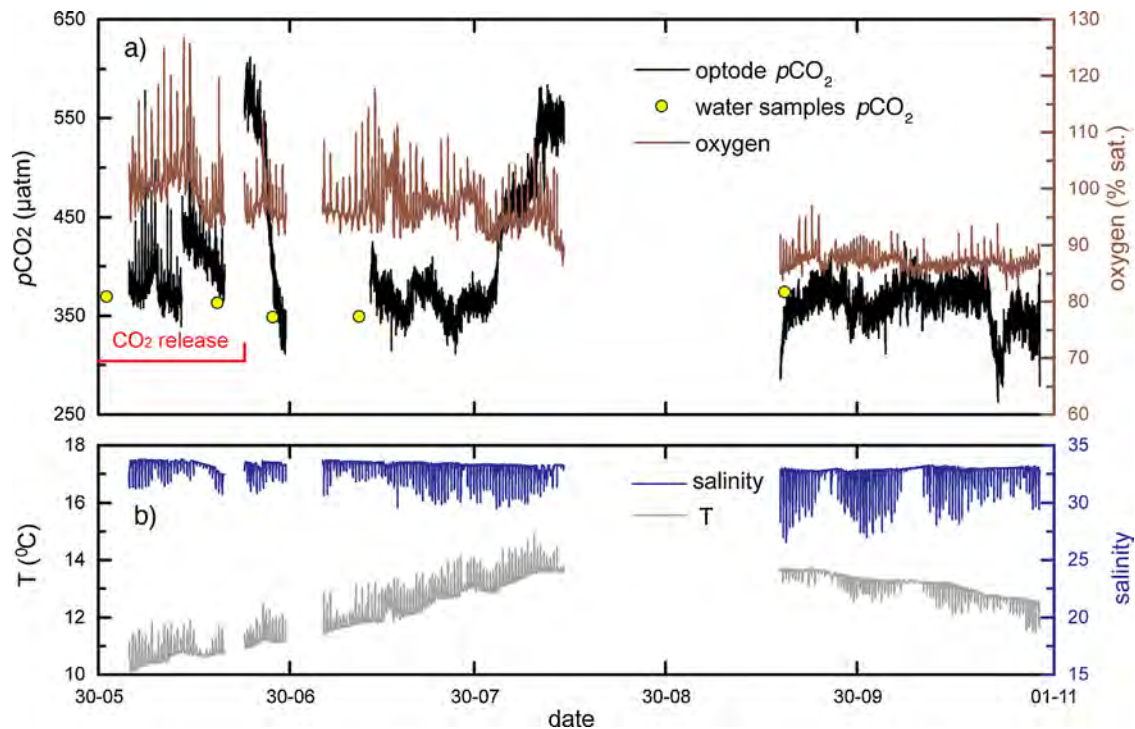


Fig. 4. Seaguard® data over June–October 2012. (a) $p\text{CO}_2$ and oxygen with a marked period of gas release, and (b) temperature and salinity time-series recorded at the release site (Z1). Yellow circles in (a) indicate $p\text{CO}_2$ data calculated from water samples analyzed for DIC and Ar . Gaps in the data are due to service of Seaguard® instrument or its use in a different project. (For interpretation of the references to colour in this figure legend, the reader is referred to the web version of this article.)

pattern and in the direction of the water flow, as recorded by the current meters on the Seaguard® and the RCM instruments (see Section 3.5).

3.3. Background parameters (temperature, salinity, currents and oxygen)

Results from June to October 2012, when the Seaguard® instrument was deployed, are presented in Fig. 4. The clear influence of tides is visible in most of the data. Temperature varied between 9.9 and 14.3 °C and followed the general seasonal pattern with increasing temperatures from May to August and slowly decreasing through September–October to 12.5 °C. Depending on tidal conditions temperature changed within ± 1 °C. Recorded temperature time-series showed negative spikes at low tide during September–October, and positive spikes during June–August, meaning higher temperature at the surface during summer.

Salinity varied between 25.7 and 33.8 with tidally induced salinity oscillations in the order of 1–5, and with higher amplitudes during the final September–October deployment. It is worth to notice that water in Ardmucknish Bay was freshening by river discharge, and salinity gradually decreased from 33.4 to 32.5 during June–October (Fig. 4b)

Currents were strongly affected by the tidal circulation. They varied between 0 and 40.5 cm/s with an overall average of 3.3 cm s^{-1} . The relatively weak average current speed reflects the position of the instrument close to the bottom. The Doppler Current Sensor of the Seaguard® was positioned about 40 cm above the seabed, which is likely to be close to the logarithmic boundary layer. The two other recording current meters (Table 1) were positioned in frames ~ 80 cm above the seabed. These instruments recorded somewhat higher average current speeds, 4.8 cm s^{-1} (RCM#643) and 3.6 cm s^{-1} (RCM#419) respectively, from May–September. Measurements from the current meters were used to calibrate and validate the circulation model used in this study.

Oxygen varied between 60% and 127% air saturation (Fig. 4a) in the bottom water. Especially in the beginning of June a combination of tides and primary production/consumption could lead to 40% changes in air saturation in some hours. There was a general decrease in the average air saturation from $\sim 105\%$ in the beginning of June to $\sim 85\%$ in the end of October.

Oxygen saturation time-series during post-injection period showed moderate daily oscillations correlating with tidal circulation in the bay. The amplitude of these oscillations were higher during June–August, governed by primary production and availability of solar radiation at that period. In September–October the amplitude of oscillations was two to three times lower, and mainly controlled by temperature changes at the bottom due to tidal circulation. At that period, surface water was colder than near the bottom, implying lower temperature and higher oxygen concentration at low tide.

3.4. Multivariate analysis

PCA analysis of the collected data showed a poor correlation between weather parameters, such as wind speed and direction, precipitation, PAR and air temperature, and variations in $p\text{CO}_2$, oxygen, salinity, temperature, currents in the bottom water and tidal activity. Hence weather data was excluded from further evaluation.

A supervised PLS model for each of the five Seaguard® deployments in Z1 (Table 1) showed correlation between the variations of oxygen and $p\text{CO}_2$ in particular, and between the variations of oxygen and $p\text{CO}_2$ and the other measured parameters (salinity, temperature and tides) in general. At the time when the Seaguard® was deployed at the epicentre (Seaguard.D1, .D2, .D4-release) of gas release, a strong correlation between peaks in $p\text{CO}_2$ and low tide was observed, and appeared as equally distanced from origo (centre point) variables in the scatter plot (Fig. 7a). No clear correlation in the pair $p\text{CO}_2$ –oxygen was identified when the external source of CO_2 was in operation during gas release.

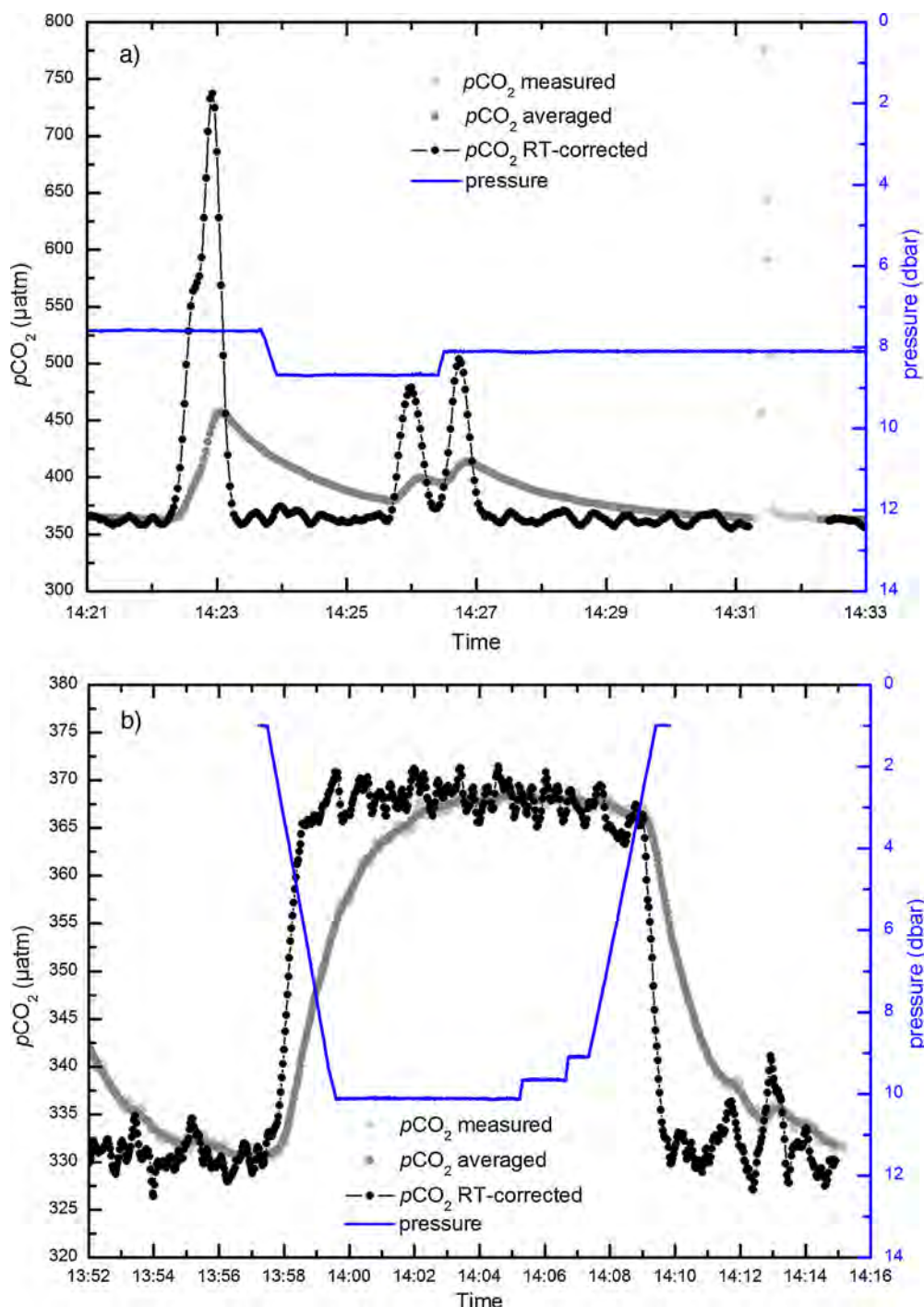


Fig. 5. $p\text{CO}_2$ data obtained from the HydroC™ along with depth information (a) while drifting over the release area Z1 on day 36 and (b) after the gas release ended on day 41. Note the different scales for $p\text{CO}_2$. In both plots the processed measured $p\text{CO}_2$ signal is shown along with the averaged data (moving average of approx. 12 s within the upper plot and approx. 30 s within the lower plot respectively) that served as an input to the iterative determination of the response time (RT) corrected $p\text{CO}_2$ time-series.

Multivariate analysis of post-injection deployments (Seaguard.D4-D6), in contrary, revealed a clear negative correlation between $p\text{CO}_2$ and oxygen variations, while connection to the tidal cycle weakened (Fig. 7b).

3.5. Water circulation in Ardmucknish Bay: recorded velocity regime

The dominating circulation pattern at the release site is determined by a combination of coastline, bathymetry, tides and, to a

lower extent, by the wind pattern. A jet current heading toward the NW coast of the Ardmucknish bay is formed at each tidal cycle on the ebb stage. When the leading edge of the tidal 'bora' (a train of internal waves set at the tidal front) reaches shallower water the flow splits into a pair of smaller cyclonic and antic-cyclonic 'eddies', which decay when approaching the opposite shore.

The progressive vector diagrams calculated from the velocity records of the three current meters deployed at different distances from the impact site Z1 demonstrate the shift in direction and smaller variations in intensity of the general flow, which confined

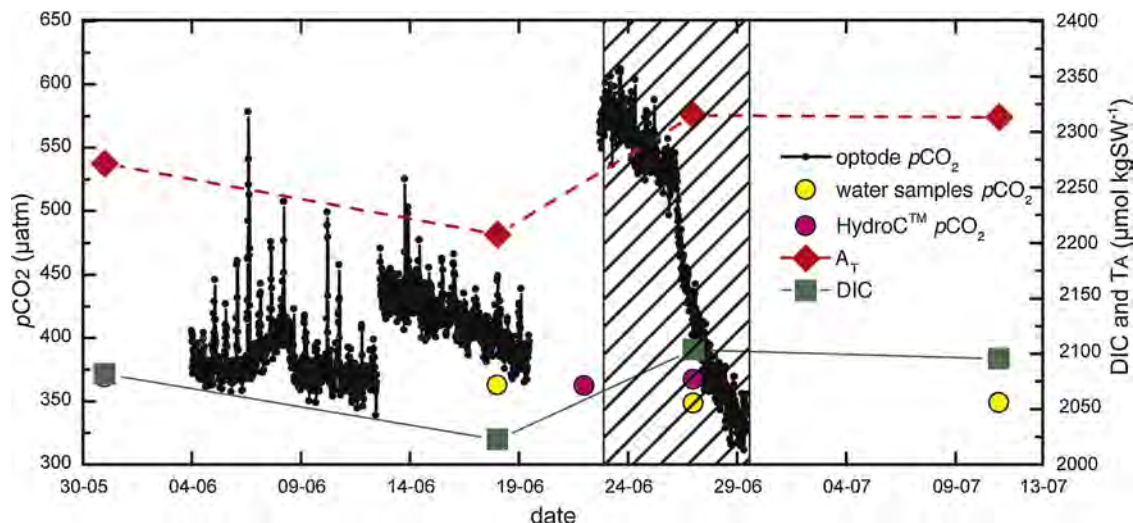


Fig. 6. $p\text{CO}_2$ time-series recorded by optode during the release of CO_2 and until the recovery (shaded area) of the water column. Water samples $p\text{CO}_2$ values derived from DIC/A_T (yellow) and measured by HydroCTM 1 m above the bottom (cyan) represent background levels. DIC and A_T analyzed from water samples are plotted for better understanding of recovery pattern shown by $p\text{CO}_2$ optode. Shaded area shows recovery period in the water column. (For interpretation of the references to colour in this figure legend, the reader is referred to the web version of this article.)

in time with the relocation of the instruments (Fig. 8a and Table 2). The changes in the circulation pattern and velocity records also correlated with wind velocities maps at 10 m height over Ardmucknish Bay (Supplementary material).

Long-term deployment data from the RCMs and Seaguard[®] (June 6th–October 28th) confirmed what was found with the short-term record analyses: at Z4 the velocity vector rotation was predominantly counter clockwise (CCW) cyclonic. At both the near source sites Z3 and Z1, the velocity vector rotation was clockwise (CW) anti-cyclonic.

The Seaguard[®] current profiler registered several occasions with sudden changes in the main flow. Between July 5th and July 27th the flow was predominantly towards NE. On July 28th it changed its direction by $\sim 180^\circ$ towards SW until July 31st. From August 1st to August 12th it changed again towards ENE gradually veering towards E. From the recorded $p\text{CO}_2$ time-series (Fig. 4a) it is seen that the latter change in circulation coincided in time with the two-step elevation in $p\text{CO}_2$ values compared to the baseline.

4. Discussion

4.1. Detection of CO_2 release

The QICS CO_2 release experiment proved to be challenging, but yet feasible in terms of chemically detecting the signal from and

describing the distribution of the released CO_2 , escaping from the seabed into the overlying water column.

The distribution of gaseous and dissolved CO_2 in the water column was heterogeneous in both time and space during the release with bubble-streams regularly shifting location within the limited ‘footprint’ of the release (Cevaloglu et al., in this issue) and also varying in intensity with the hydrostatic pressure (Fig. 3a and b; Blackford et al., 2014). The complex hydrodynamic environment typical for coastal- and continental-shelf settings made it even more challenging to clearly capture the CO_2 signal of the injected gas.

Using standard techniques, such as occasional ship-based discrete water sampling, it was almost impossible to capture and describe established gradients in $p\text{CO}_2$. Due to the lack of temporal coverage and low spatial precision water sampling appeared to be insufficient to detect the leakage of CO_2 , however it was required to quality assure and calibrate the $p\text{CO}_2$ optode and ISFET- $p\text{CO}_2$ sensor *in situ*. Agreement between optode data and reference values from water samples confirmed stability and reliability of the $p\text{CO}_2$ optode measurements (Fig. 4a), and hence the robustness of this relative new technology.

Continuous *in situ* measurements in contrast to discrete sampling reflected the real dynamics and heterogeneity of $p\text{CO}_2$ distribution as a result of sub-seabed emissions during and after the actual release to the water column. Only 15% of the injected CO_2 escaped the sediment-water interface as gas bubbles at the

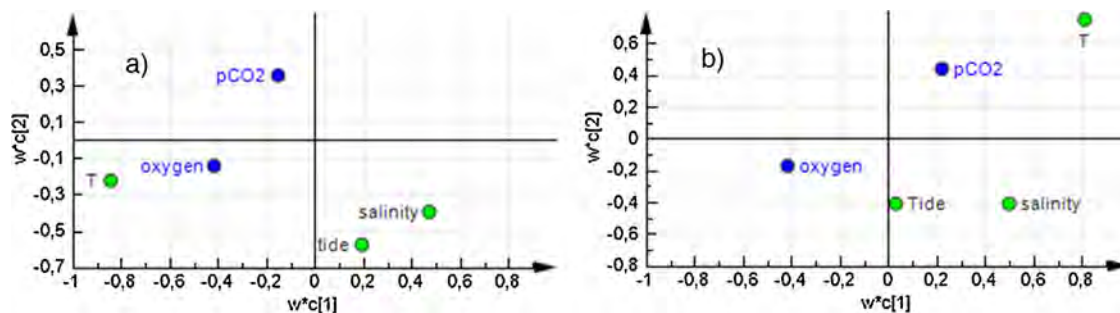


Fig. 7. Graphic representation of PLS model applied in multivariate analysis of the collected data: scatter plot of the Y ($p\text{CO}_2$ and oxygen) and X (T, salinity, tide) weights. Axes represent first ($w \times c[1]$) and second vector component ($w \times c[2]$) of the correlations between the variables. (a) Period with CO_2 release. (b) Period without CO_2 release. The plots show the relation between Y variables and X variables, and the relation within Y's and X's. Points in the opposite corners and distanced far away from origo (centre point – crossing of the axes) indicate strong negative correlation between the variables. Points that are closer to the centre have weaker influence on the model.

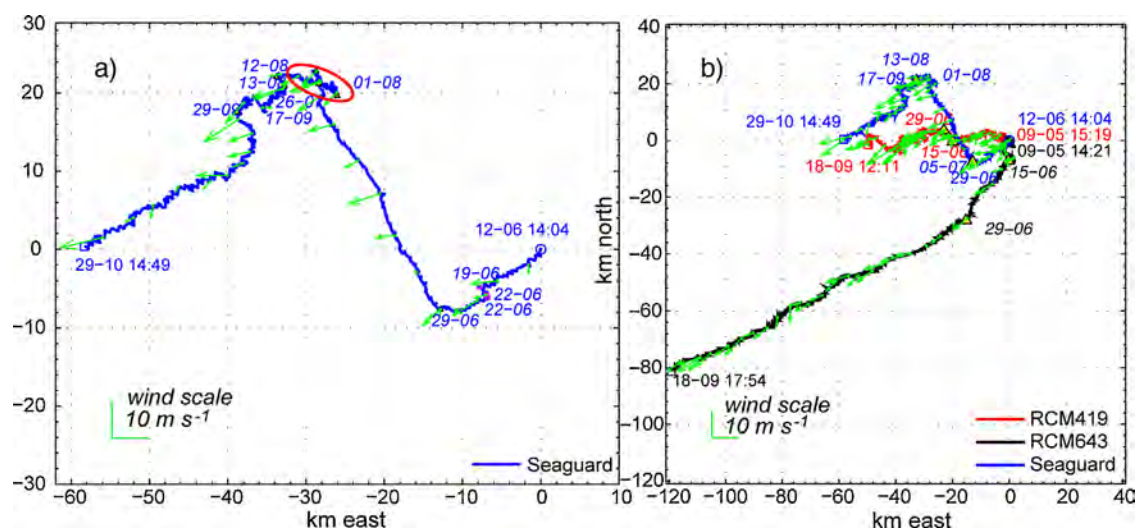


Fig. 8. Predominant water flow direction recorded by the current meters: (a) details of Seaguard® data and (b) overview of Seaguard® and RCM9 instruments deployed in Ardmucknish Bay in May/June–October 2012. Dates indicate relocation/redeployment of the instrument or change in flow direction. The red oval at (a) indicate the change in flow direction between August 1st and August 12th. Three-daily average wind direction from the Dunstaffnage weather station is indicated with green arrows (For interpretation of the references to colour in this figure legend, the reader is referred to the web version of this article.).

highest injection rate ($210 \text{ kg CO}_2 \text{ d}^{-1}$); with the remaining 85% still captured within the sediments, either as gas bubbles or dissolved in the porewater (Blackford et al., 2014). These numbers are consistent with some estimates of chronic CO_2 leakages, e.g. via abandoned well bores. The released amounts of CO_2 are a small fraction of what can be expected during real-life acute leaks minding realistic sizes of potential CCS. Nevertheless, the horizons of sharp concentration gradients are detectable by means of high-temporal observations of $p\text{CO}_2$ evolution at different levels above the bottom and different distances from the emission site.

In close vicinity to the pockmarks, i.e. where the gas bubble streams enter the water column, tidally driven oscillations in the $p\text{CO}_2$ had the highest amplitude as detected by the ISFET- $p\text{CO}_2$ sensor. Dissolution of gas bubbles as they ascend in the water column was described to control distribution of $p\text{CO}_2$ in a vertical plane (Dissanayake et al., 2012; Dewar et al., 2013). Elevated $p\text{CO}_2$ values in the near-bottom masses were further enhanced by mixing of CO_2 -saturated pore water, which escapes from pockmarks together with the gas stream. As a result, observed $p\text{CO}_2$ peaks reached up to $1250 \mu\text{atm}$ at low tide with occasional values of $\sim 1600 \mu\text{atm}$. Weak bottom currents and density gradients prevented efficient mixing and restricted upwelling of the denser CO_2 saturated bottom water in favour of horizontal spreading.

At 30 cm above the seafloor, the $p\text{CO}_2$ optode registered peak concentrations of $580 \mu\text{atm}$ and a horizontal gradient equal to $\pm 80\text{--}100 \mu\text{atm } p\text{CO}_2$ after relocation for $\sim 1 \text{ m}$ (Fig. 3c). This was interpreted as evidence of strong spatial variability at the release site where the outflowing gas could take different routes through the water column depending on the variable hydrography and/or re-establishing of gas chimneys with a new tidal cycle. After the Seaguard® was moved some of the tidal night-time peaks in oxygen became more distinguished confirming that water column conditions changed after relocation (Fig. 3c).

Occasional $p\text{CO}_2$ peaks with high values in the order of $540\text{--}740 \mu\text{atm}$, detected during 2D-mapping of the release site with the HydroC™ sensor (Fig. 5a), pointed on the existence of microenvironments around each focused bubble stream, similar to what is observed in a close vicinity to pockmarks. The 'footprint' area of $\sim 30 \text{ m}$ in diameter was verified by HydroC™ when drifting over Z1 (Fig. 5a). Since at the given vessel speed of $\sim 0.1 \text{ knts}$ a temporal interval of 1 min correlates with a spatial extend of

$\sim 3 \text{ m}$, 10 min interval in-between the peaks detected by HydroC™ (Fig. 5a) translates into $\sim 30 \text{ m}$ long area of the transect. This indicated dispersion in the water column, which was limited to the restricted area of focused flow of CO_2 bubble plumes, although with a slightly shifting position controlled by tidal conditions and hydrography. In this context, high temporal resolution $p\text{CO}_2$ data and response time correction algorithms as applied within the profiling and drifting measurements of the HydroC™ proved to be a useful and powerful observation method. Distinct $p\text{CO}_2$ peaks on a sub minute time scale with recoveries back to baseline in between could be obtained (Fig. 5a) as well as depth profiles clarified (Fig. 5b).

Increasing flow rates appeared to have minor influence on the baseline values from optode and ISFET- $p\text{CO}_2$ except at the very end when the flow rates were finally increased to $210 \text{ kg CO}_2 \text{ d}^{-1}$. The intensified CO_2 flow from the seabed further enhanced stratification of the water column, resulting in more pronounced differences in baseline values recorded ~ 3 and $\sim 30 \text{ cm}$ above the seafloor, i.e. 1200 and $570 \mu\text{atm}$, respectively. The values measured $\sim 3 \text{ cm}$ above the bottom seemed to represent a microenvironment created by a gas chimney at the pockmark, rather than background $p\text{CO}_2$ value in the water column. The seismic data confirmed that gas chimneys were fully developed all the way up to the sediment–water interface only towards the end of the release phase (Cevatoglu et al., in this issue). The higher, but narrower peaks were observed during spring tides and lower, but broader peaks during neap tides. In the latter case the difference in hydrostatic pressure was lower, which allowed $p\text{CO}_2$ peaks to fully develop in-between the tidal changes.

Observations and measurements done in this study are unique in that it was a first attempt to assess the impacts of purposefully released CO_2 in the water column by imitating real-life leakages from CCS. A natural analogue of 'failed' CCS, Panarea site, Southern Italy, is well described in terms of the impacts of leaked CO_2 on seawater chemistry (Pearce et al., 2014). The natural release of CO_2 , however, is occurring in much larger quantities than the controlled CO_2 release within the QICS. Observed peak concentrations in order of $1600 \mu\text{atm}$ in this study, are much smaller compared to peak concentrations of 4.5% CO_2 (or $45000 \mu\text{atm}$) at Panarea. Baseline $p\text{CO}_2$ values of $\sim 2000 \mu\text{atm}$ and $\sim 6000 \mu\text{atm}$ were observed right above the epicentre at Panarea site at moderate and high CO_2

flux rates, respectively. Higher CO₂ fluxes facilitated much stronger vertical and horizontal gradients of pCO₂ distribution, which could be detected, unlike during the QICS experiment, by means of discrete water sampling along the transect. Observations of natural CO₂ leaking sites emphasize the effect of seasonal variability and hydrography both on concentration and distribution of CO₂ gas in the water column (Pearce et al., 2014), which have to be taken into consideration when designing a suitable monitoring strategy for future CCS.

4.2. Recovery after CO₂ release

After the gas release was shut off, pCO₂ in the bottom water recovered within 7 days according to the pCO₂ optode. The towed HydroC™ measurements, 1 m above the bottom on day 41, did not show any areas of elevated pCO₂ either. A gradual build-up of DIC and A_T in the water column was tracked by simultaneous decrease of pCO₂ levels for ~1 week after the termination of the release, where after all three parameters seemed to have reached equilibrium (Fig. 6).

Observed changes in carbonate chemistry are presumably a combination of natural forcing and flux out of the sediment, where the highest DIC concentrations were measured in the near-surface sediments after the injection was stopped (Blackford et al., 2014; Lichtschlag et al., in this issue). Pore water concentrations of DIC and A_T remained high even though the water column data indicated full recovery at day 41. The pore water chemistry (DIC and A_T) had returned to background concentrations three weeks after the termination of the CO₂ release, most likely through precipitation of CaCO₃ or through physical or biological advection of pore waters (Blackford et al., 2014).

Data from the ISFET-pCO₂ sensor indicated low values and a fast (<2 days) recovery pattern, which is further discussed in Shitashima et al. (in this issue).

4.3. Multivariate data analysis

The multivariate analysis of data turned out to be an efficient tool in distinguishing between periods with and without anthropogenic release. It was shown that in highly dynamic waters like Ardmucknish Bay natural variability is comparable in its levels of pCO₂ variation with the effects of an external CO₂ source (Fig. 4a). Natural forcing, such as biological respiration and exchange of water masses, may be a stronger factor in carbonate system dynamics than the effect of a small acute CO₂ release. We addressed this problem by applying a multivariate analysis technique and looked specifically for the strongest correlation. During the CO₂ release phase, the strongest dependence was found between peaks in pCO₂ and low tide – which agreed with the observations of lack of bubble streams during high tide. During the recovery phase, however, multivariate analysis indicated strong negative correlation between the variations of pCO₂ and oxygen, implying that natural factors were now driving the changes in concentrations of these two gases. The external source of CO₂ was breaking the natural correlation between pCO₂ and oxygen.

4.4. Hydrographical conditions

In general, the circulation in Ardmucknish Bay is tidally driven and the influence of tidal circulation was significant on all the measured parameters. In addition the water depth at the release site was ca. 10–12 m, allowing light penetration all the way to the bottom. This led to enhanced oxygen variations due to benthic activity: primary production and super saturation of oxygen in bottom water during spring/summer days, and respiration during nights, which consumes oxygen (Fig. 4a).

From the observations of pCO₂, main current velocity and velocity vector rotation data, we can conclude that a change in flow direction at Z1 could (a) enhance/inhibit clockwise (CW) anti-cyclonic velocity rotation, and (b) affect water renewal at the site. If the change in flow direction facilitates velocity rotation, this should result in quasi-stationary eddy-like structures, which decay and emerge with every tidal cycle. These structures may increase the normal residence time of water and hence increase level pCO₂ at the site. If the flow direction facilitates renewal of the water with each tidal cycle, this would counteract, in our case, the clockwise anti-cyclonic rotation so that normal eddies lose their velocity, and would stop the rise of pCO₂. At the release site there were several periods of cyclonic circulation, e.g. in the beginning of August (Fig. 8b), which increased the water residence time, and led to occasional increases in pCO₂ levels.

5. Conclusions

This work is focused on the technical challenges of detecting anthropogenic CO₂ leakages from a simulated sub-seabed CO₂ storage site using instrumentation installed in the overlying bottom water. Data provided by three different types of pCO₂ sensors in combination with other chemical and physical sensors measuring water column conditions are presented and discussed in this paper.

The results showed that the purposefully released CO₂ caused tidally-induced pCO₂ oscillations in the water column of Ardmucknish Bay in the order of 30–1250 μatm and resulted in a gradual build-up of the background level of pCO₂, from 369 μatm at the beginning up to ~570 μatm close to the seafloor, when the observed gas flow at the sediment–water interface was the most intense, (i.e. at the injection rate of 220 kg CO₂ d⁻¹). The release caused strong spatial heterogeneity of pCO₂ above the epicentre detected by (a) two sensors measuring within 1 m from each other, i.e. one optical pCO₂ and one ISFET-pCO₂ sensor, (b) by comparing mentioned devices' data with a 2D horizontal pCO₂ map recorded by a third, NDIR-based pCO₂ sensor, a HydroC™ CO₂, and (c) by relocation of the pCO₂ optode during redeployment. Acidification as a result of CO₂ dissolution in the water column and the sediment was temporary; the recovery took <7 days and <22 days, respectively for water and sediment, until the system returned to its original natural state.

This study demonstrates that detection of CO₂ leakage from an anthropogenic storage site is possible, but challenging. An aspect of strong heterogeneity of the distribution of the CO₂ gas bubble stream and of the associated dissolved CO₂ species should be taken into consideration as well as a localized 'footprint' of the release as detected in the study.

CCS would most likely be situated at deeper sites with less variable water conditions than at the hydrographically complex system of Ardmucknish Bay. Working in Ardmucknish Bay introduced an additional challenge by bringing more uncertainty to identifying changes associated with CO₂ leakages in contrary to those associated with natural coastal processes. However, CCS might as well happen at the shelves and pipelines will transverse the shore and coastal regions, initially in very shallow water with the conditions similar to this study. At identified CCS sites with minor currents, small tidal influences and moderate gas fluxes through a larger seabed area one should expect more pronounced effects of CO₂ leaks in the form of an increased background pCO₂ level and less pronounced gradients close to the leak. Hence, the detection with permanently deployed sensors measuring pCO₂/pH/O₂ with high sensitivity is suggested as a feasible solution for the targeted areas near the hotspots, such as injection wells, pipelines, and other places of higher risks (e.g. known faults). Depending on the size of the sub-seabed geological storage, a few AUV or towed systems

equipped with sensor packages, described in this paper and in Blackford et al. (2014), should be deployed to scan larger areas on regular intervals. As highlighted in this study, response time of the instruments should be carefully addressed by introducing a correction for signal variation over time. This is applicable for both fixed and movable monitoring platforms. Treatment of incoming data and further assessing the probability of leakage should be done on-line in a framework of multivariate data analysis. This approach decreases risks of misinterpretation of the data caused by e.g. confusing natural variability with an actual leakage.

Considerations listed above are based on the results from this study and well-known facts about biogeochemistry of the water column and sediments, and should not be applied directly for designing the monitoring strategies for CCS in general. In contrary, our results emphasize the necessity of a unique approach to each potential storage site depending on e.g. water depth, bathymetry, etc., and solid knowledge about hydrological and biogeochemical conditions before the storage becomes operational.

Acknowledgements

This work was financially supported by SENSEnet (International sensor development network) – a Marie Curie Initial Training Network (ITN) funded by the European Commission Seventh Framework Program under contract number PITN-GA-2009-237868. We thank the UK National Environmental Research Council (NERC) and Scottish Government for kindly providing funding to the QICS project (NE/H013911/1). We also acknowledge the Lochnell Estate and Tralee Bay Holiday Park for providing on land site access, the divers at the National Facility of Scientific Diving (NFS) and the crew on R/V Seol Mara at SAMS for deploying and recovering the instruments. We would like to thank Rachael James and Doug Connelly from the National Oceanography Centre (NOC) in Southampton for seawater sample analysis of DIC and A_T as well as providing background CTD and currents data for the modelling.

Appendix A. Supplementary data

Supplementary data associated with this article can be found, in the online version, at [doi:10.1016/j.ijggc.2014.10.021](https://doi.org/10.1016/j.ijggc.2014.10.021).

References

Aleynik, D., Stahl, H., Inall, M., 2012. The HYPOX D2.4 Report on oxygen dynamics in silled basins and its dependence on boundary conditions (accessed 05.06.13.).
Atamanchuk, D., Tengberg, A., Thomas, P.J., Hovdenes, J., Apostolidis, A., Huber, C., et al., 2014. Performance of a lifetime-based optode for measuring partial pressure of carbon dioxide in natural waters. *Limnol. Oceanogr. Methods* 12, 63–73, [http://dx.doi.org/10.4319/lom.2014.12.63](https://dx.doi.org/10.4319/lom.2014.12.63).
Blackford, J.C., Jones, N., Proctor, R., Holt, J., 2008. Regional scale impacts of distinct CO₂ additions in the North Sea. *Mar. Pollut. Bull.* 56 (8), 1461–1468, [http://dx.doi.org/10.1016/j.marpolbul.2008.04.048](https://dx.doi.org/10.1016/j.marpolbul.2008.04.048).
Blackford, J.C., Torres, R., Cazanave, P., Artioli, Y., 2013. Modelling dispersion of CO₂ plumes in sea water as an aid to monitoring and understanding ecological impact. *Energy Procedia* 37, 3379–3386, [http://dx.doi.org/10.1016/j.egypro.2013.06.226](https://dx.doi.org/10.1016/j.egypro.2013.06.226).
Blackford, J.C., Stahl, H., Bull, J.M., Berges, B.J.P., Cevatoglu, M., Lichtschlag, A., et al., 2014. Detection and impacts of leakage from sub-seafloor deep geological carbon dioxide storage. *Nat. Clim. Change* 4, 1011–1016, [http://dx.doi.org/10.1038/nclimate2381](https://dx.doi.org/10.1038/nclimate2381).
Brewer, P.G., 2003. Direct injection of carbon dioxide into the oceans. In: *The Carbon Dioxide Dilemma: Promising Technologies and Policies*. National Academies Press, Washington, D.C., pp. 43–51.
Brewer, P.G., Peltzer, E.T., Aya, I., Haugan, P., Bellerby, P., Yamane, K., et al., 2004. Small scale field study of an ocean CO₂ plume. *J. Oceanogr.* 60, 751–758, [http://dx.doi.org/10.1007/s10872-004-5767-9](https://dx.doi.org/10.1007/s10872-004-5767-9).
Caramanna, G., Voltattorni, N., Maroto-Valer, M., 2011. Is Panarea Island a valid and cost-effective natural laboratory for the development of detection and monitoring techniques for submarine CO₂ seepage? *Greenh. Gases: Sci. Technol.* 1 (3), 200–210, [http://dx.doi.org/10.1002/ghg.28](https://dx.doi.org/10.1002/ghg.28).
Cevatoglu, M., Bull, J.M., Vardy, M.E., Gernon, T.M., Wright, I.C., Long, D. First controlled sub-seabed CO₂ release experiment in Ardmucknish Bay, Oban: Insights

into gas migration pathways from seismic reflection data and impacts on sediment physical properties (in this issue).
Chen, C., Liu, H., Beardsley, R.C., 2003. An unstructured grid, finite-volume, three dimensional, primitive equations ocean model: application to coastal ocean and estuaries. *J. Atmos. Ocean. Technol.* 20, 159–186, [http://dx.doi.org/10.1175/1520-0426\(2003\)020<0159:AUGFVT>2.0.CO;2](https://dx.doi.org/10.1175/1520-0426(2003)020<0159:AUGFVT>2.0.CO;2).
Dewar, M., Wei, W., McNeil, D., Chen, B., 2013. Small-scale modelling of the physico-chemical impacts of CO₂ leaked from sub-seabed reservoirs or pipelines within the North Sea and surrounding waters. *Mar. Pollut. Bull.* 73 (2), 504–515, [http://dx.doi.org/10.1016/j.marpolbul.2013.03.005](https://dx.doi.org/10.1016/j.marpolbul.2013.03.005).
Dickson, A.G., Afghan, J.D., Anderson, G.C., 2003. Reference materials for oceanic CO₂ analysis: a method for the certification of total alkalinity. *Mar. Chem.* 80, 185–197, [http://dx.doi.org/10.1016/S0304-4203\(02\)00133-0](https://dx.doi.org/10.1016/S0304-4203(02)00133-0).
Dissanayake, A., DeGraff, J.A., Yapa, P.D., Nakata, K., Ishihara, Y., Yabe, I., 2012. Modelling the impact of CO₂ releases in Kagoshima Bay, Japan. *J. Hydro-Environ. Res.* 6 (3), 195–208, [http://dx.doi.org/10.1016/j.jher.2012.02.001](https://dx.doi.org/10.1016/j.jher.2012.02.001).
Fiedler, B., Fietzek, P., Vieira, N., Silva, P., Bittig, H.C., Körtzinger, A., 2013. In situ CO₂ and O₂ measurements on a profiling float. *J. Atmos. Ocean. Technol.* 30, 112–126, [http://dx.doi.org/10.1175/JTECH-D-12-00043.1](https://dx.doi.org/10.1175/JTECH-D-12-00043.1).
Fietzek, P., Fiedler, B., Steinhoff, T., Körtzinger, A., 2014. In situ quality assessment of a novel underwater pCO₂ sensor based on membrane equilibration and NDIR spectrometry. *J. Atmos. Ocean. Technol.* 31 (1), 181–196, [http://dx.doi.org/10.1175/JTECH-D-13-00083.1](https://dx.doi.org/10.1175/JTECH-D-13-00083.1).
Gough, C., Shackley, S., (Eds.), 2005. An integrated assessment of carbon dioxide capture and storage in the UK, Tyndall Centre Tech. Rpt. 47 (<http://www.tyndall.ac.uk/sites/default/files/t2.21.pdf>).
Hall-Spencer, J.M., Rodolfo-Metalpa, R., Martin, S., Ransome, E., Fine, M., Turner, S.M., et al., 2008. Volcanic carbon dioxide vents show ecosystem effects of ocean acidification. *Nature* 454, 96–99, [http://dx.doi.org/10.1038/nature07051](https://dx.doi.org/10.1038/nature07051).
Haszeldine, R.S., 2009. Carbon capture and storage: how green can black be? *Science* 325 (5948), 1647–1652, [http://dx.doi.org/10.1126/science.1172246](https://dx.doi.org/10.1126/science.1172246).
Jeong, S., Sato, T., Chen, B., Tabeta, S., 2010. Numerical simulation on multi-scale diffusion of CO₂ injected in the deep ocean in a practical scenario. *Int. J. Greenh. Gas Control* 4 (1), 64–72, [http://dx.doi.org/10.1016/j.ijggc.2009.09.021](https://dx.doi.org/10.1016/j.ijggc.2009.09.021).
Kano, Y., Sato, T., Kita, J., Hirabayashi, S., Tabeta, S., 2009. Model prediction on the rise of pCO₂ in uniform flows by leakage of CO₂ purposefully stored under the seabed. *Int. J. Greenh. Gas Control* 3 (5), 9, [http://dx.doi.org/10.1016/j.ijggc.2009.03.004](https://dx.doi.org/10.1016/j.ijggc.2009.03.004).
Kano, Y., Sato, T., Kita, J., Hirabayashi, S., Tabeta, S., 2010. Multi-scale modelling of CO₂ dispersion leaked from seafloor off the Japanese coast. *Mar. Pollut. Bull.* 60 (2), 215–224, [http://dx.doi.org/10.1016/j.marpolbul.2009.09.024](https://dx.doi.org/10.1016/j.marpolbul.2009.09.024).
Kirkwood, W., Graves, D., Conway, M., Pargett, D., Scholfield, J., Walz, P., et al., 2005. Engineering development of the free ocean CO₂ enrichment (FOCE) experiment. *MTS/IEEE Oceans*, [http://dx.doi.org/10.1109/OCEANS.2005.1640013](https://dx.doi.org/10.1109/OCEANS.2005.1640013) (MTS/IEEE #050304–93).
Kirkwood, W., Peltzer, E.T., Walz, P., Brewer, P., 2009. Cabled observatory technology for ocean acidification research. *Ocean* 2009–Eur. 1 (6), 11–14, [http://dx.doi.org/10.1109/OCEANSE.2009.5278337](https://dx.doi.org/10.1109/OCEANSE.2009.5278337).
Lewis, E., Wallace, D.W.R., 1998. Program Developed for CO₂ System Calculations. Carbon Dioxide Information Analysis Center, Oak Ridge National Laboratory, U.S. Department of Energy, Oak Ridge (TN) (ORNL/CDIAC-105).
Lichtschlag, A., James, R.H., Stahl, H., Connelly, D. Effect of a controlled sub-seabed release of CO₂ on the biogeochemistry of shallow marine sediments, their porewaters, and the overlying water column (in this issue).
Martz, T.R., Connerly, J.G., Johnson, K.S., 2010. Testing the Honeywell Durafet® for seawater pH applications. *Limnol. Oceanogr. Methods* 8, 172–184, [http://dx.doi.org/10.4319/lom.2010.8.172](https://dx.doi.org/10.4319/lom.2010.8.172).
Miloshevich, L.M., Paukkunen, A., Vömel, H., Oltmans, S.J., 2004. Development and validation of a time-lag correction for vaisala radiosonde humidity measurements. *J. Atmos. Ocean. Technol.* 21 (9), 1305–1327, [http://dx.doi.org/10.1175/1520-0426\(2004\)021<1305:DAVOT>2.0.CO;2](https://dx.doi.org/10.1175/1520-0426(2004)021<1305:DAVOT>2.0.CO;2).
Pearce, J., Blackford, J., Beaubien, S., Foekema, E., Gemeni, V., Gwosdz, S., et al., 2014. A guide to potential impacts of leakage from CO₂ storage. D5.2b, revision 5. EU project RISCs.
Saderne, V., Fietzek, P., Herman, P.M.J., 2013. Extreme variations of pCO₂ and pH in a macrophyte meadow of the Baltic Sea in summer: evidence of the effect of photosynthesis and local upwelling. *PLoS One* 8 (4), e62689, [http://dx.doi.org/10.1371/journal.pone.0062689](https://dx.doi.org/10.1371/journal.pone.0062689).
Shitashima, K., Kyo, M., 1998. Application of chemical sensor to oceanography—development of deep sea pH sensor using ISFET. *Chikyukagaku (Geochem.)* 15, 1–11 (in Japanese with English abstract).
Shitashima, K., Kyo, M., Koike, Y., Henmi, H., 2002. Development of in-situ pH sensor using ISFET. In: *Proceedings of the 2002 International Symposium on Underwater Technology*, [http://dx.doi.org/10.1109/UT.2002.1002403](https://dx.doi.org/10.1109/UT.2002.1002403) (IEEE/O2EX556:106–8).
Shitashima, K., Maeda, Y., Koike, Y., Ohsumi, T., 2008. Natural analogue of the rise and dissolution of liquid CO₂ in the ocean. *Int. J. Greenh. Gas Control* 2 (1), 95–104, [http://dx.doi.org/10.1016/S1750-5836\(07\)00092-8](https://dx.doi.org/10.1016/S1750-5836(07)00092-8).
Shitashima, K., 2010. Evolution of compact electrochemical in-situ pH-pCO₂ sensor using ISFET-pH electrode. *Oceans* 1 (4), 20–23, [http://dx.doi.org/10.1109/OCEANS.2010.5663782](https://dx.doi.org/10.1109/OCEANS.2010.5663782) (MTS/IEEE Seattle).
Shitashima, K., Maeda, Y., Ohsumi, T., 2013. Development of detection and monitoring techniques of CO₂ leakage from seafloor in sub-seabed CO₂ storage. *Appl. Geochem.* 30, 114–124, [http://dx.doi.org/10.1016/j.apgeochem.2012.08.001](https://dx.doi.org/10.1016/j.apgeochem.2012.08.001).
Shitashima, K., Maeda, Y., Sakamoto, A. Detection and monitoring of leaked CO₂ through sediment, water column and atmosphere in sub-seabed CCS experiment (in this issue).

- Taylor, P., Stahl, H., Blackford, J., Vardy, M.E., Bull, J.M., Akhurst, M., et al. A novel sub-seabed CO₂ release experiment informing monitoring and impact assessment for geological carbon storage (in this issue).
- Tengberg, A., Hovdenes, J., Andersson, J.H., Brocandel, O., Diaz, R., Hebert, D., et al., 2006. Evaluation of a lifetime based optode to measure oxygen in aquatic systems. *Limnol. Oceanogr. Methods* 4, 7–17, <http://dx.doi.org/10.4319/lom.2006.4.7>.
- Victoria, I., 2011. Measuring currents in demanding environments with a SeaGuard® RCM. Current meter conference. In: Proceedings of the 10th Conference on Current, Wave and Turbulence Measurements (CWTM), pp. 237–245, <http://dx.doi.org/10.1109/CWTM.2011.5759558>.
- Vizzini, S., Tomasello, A., Di Maida, G., Pirrotta, M., Mazzol, A., Calvo, S., 2010. Effect of explosive shallow hydrothermal vents on $\delta^{13}C$ and growth performance in the seagrass *Posidonia oceanica*. *J. Ecol.* 98, 1284–1291, <http://dx.doi.org/10.1111/j.1365-2745.2010.01730.x>.
- Walz, P.M., Kirkwood, W.J., Peltzer, E.T., Hester, K.C., Brewer, P.G., 2008. Creating controlled CO₂ perturbation experiments on the seafloor—development of FOCE techniques. *Oceans* 1–3, 750–753, <http://dx.doi.org/10.1109/OCEANSKOB.2008.4531025> (MTS/IEEE Kobe Techno-Ocean).
- Wilkinson, M., Haszeldine, R.S., Mackay, E., Smith, K., Sargeant, S., 2013. A new stratigraphic trap for CO₂ in the UK North Sea: appraisal using legacy information. *Int. J. Greenh. Gas Control* 12, 310–322, <http://dx.doi.org/10.1016/j.ijggc.2012.09.013>.